COMMUNICATION

Unravelling Long-lived Ligand-to-Metal Cluster Charge Transfer State in Ce-TCPP Metal Organic Frameworks

Received 00th January 20xx,
Accepted 00th January 20xx

DOI: 10.1039/x0xx00000x

*Sizhuo Yang,[a] Wenhui Hu,[a] James Nyakuchena,[a] Christian Fiankor,[c] Cunming Liu,[b] Eli Diego Kinigstein,[b] Jian Zhang,[c] Xiaoyi Zhang,[b] Jier Huang [a]**

Metal organic frameworks (MOFs) have emerged as promising photocatalytic materials for solar energy conversion. However, the fundamental understanding of light harvesting and charge separation (CS) dynamics in MOFs remain underexplored, yet they are key factors that determine the efficiency of photocatalysis. Herein, we report the design and CS dynamics of Ce-TCPP MOF using ultrafast spectroscopic methods.

The direct conversion of water or CO_2 by sun light into fuel is a promising approach to address global energy and environmental issues.[1] However, it remains a great challenge to drive such reaction in an efficient way and an appropriate catalyst is highly desired to promote the reaction in an reasonable rate. As an emerging class of porous materials, metal organic frameworks (MOFs) offer a new opportunity by taking advantage of both homogenous and heterogeneous catalysts for photocatalysis.[2] MOFs are created by assembling metal-containing secondary building units (SBUs) with organic linkers.[3] With flexible metal SBUs and organic linkers, MOFs are able to integrate light-harvesting materials and catalysts into a single matrix.[4] In addition, the high crystallinity and porous nature of MOFs may facilitate charge transport and diffusion of reactants during the photocatalytic reaction.[5] Due to these reasons, a large number of MOFs with built-in photosensitizer (PS) and molecular catalyst have been used for water splitting and CO_2 reduction.[6] However, majority of these work are centered on their catalytic performance and stability rather than fundamental mechanism. The commonly accepted catalytic pathway initiates with light absorption by the PS, which is followed by the charge separation (CS) events either through oxidative quenching of PS by electron transfer (ET) to the catalyst or reductive quenching through ET from the electron donor. As a result, it is essential to gain an intimate knowledge of the fundamental aspects of the light harvesting and CS processes before we explore MOFs for photocatalytic applications.[6c, 7] Indeed, the presence of long-lived CS state in a few MOFs following photoexcitation have been reported previously.[7a, 8] We have also reported the formation of a long-lived CS state in zeolitic imidazolate framework based on Co node and 2-methyl imidazolate ligand (ZIF-67).[9] While these fundamental studies demonstrate the great potential of MOFs as light harvesting and CS materials, these systems largely rely on the ligand which has limited absorption in visible region[7a, 8a, 8e] or the transition metal d-d transition with low extinction coefficient[9] as PS, preventing their further applications in solar energy conversion. In response to these challenges, in this work, we report the excited state and CS dynamics of a porphyrin-based Ce-TCPP MOF by optical transient absorption (OTA) and X-ray transient absorption (XTA) spectroscopy, where the TCPP ligand (tetrakis(4-carboxyphenyl)porphyrin) has broad

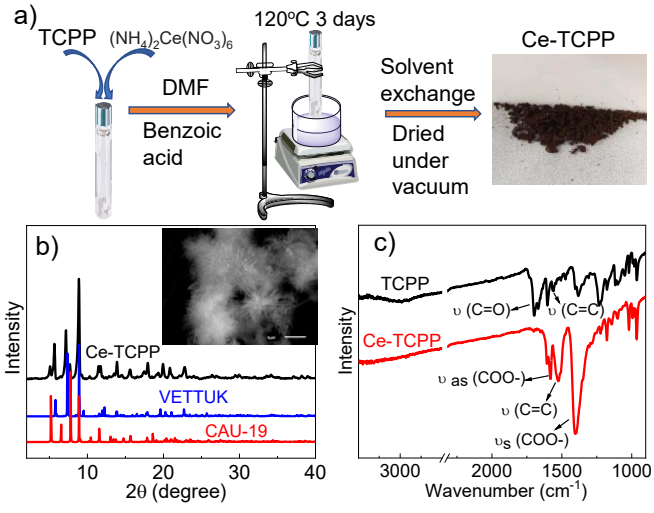

Figure 1. (a) Synthetic scheme of Ce-TCPP; (b) XRD patterns of Ce-TCPP and patterns simulated from the single crystal structure from similar TCPP MOFs; (c) FTIR spectra of TCPP and Ce-TCPP. Inset of (b) is the SEM image of Ce-TCPP MOFs.

[a] Department of Chemistry, Marquette University, Milwaukee, Wisconsin, 53201
[b] X-ray Science Division, Argonne National Laboratory, Argonne, Illinois, 60349
[c] Department of Chemistry, University of Nebraska-Lincoln, Lincoln, Nebraska, 68588

† Footnotes relating to the title and/or authors should appear here.
Electronic Supplementary Information (ESI) available: Experimental details, Figure S1-S8, Table S1-S3. See DOI: 10.1039/x0xx00000x

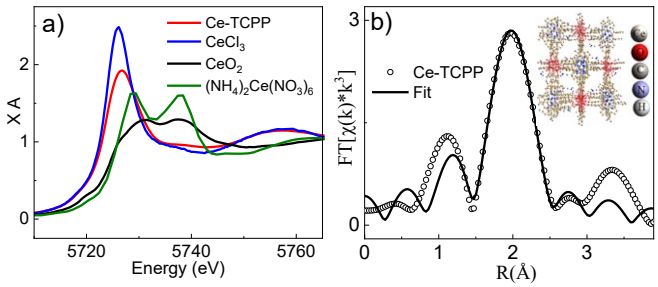

Figure 2. (a) XANES spectra of Ce-TCPP MOFs (red), $CeCl_3$ (blue), CeO_2 (black) and $(NH_4)_2Ce(NO_3)_6$ (olive). (b) The Fourier-transformed XAS spectrum of Ce-TCPP in R-space. The inset shows the fitting model. The data are shown as open dots and FEFF fits are shown as solid lines.

absorption and relatively high extinction coefficient in UV-Visible spectrum. We show that the excitation of Ce-TCPP MOFs leads to the formation of a long-lived CS state with ligand-to-metal cluster charge transfer (LCCT) character, where the mixed-phase structure in Ce-TCPP MOFs was found to play an important role in the formation of this LCCT state.

As shown in Fig. 1a, the 3D Ce-TCPP was synthesized by the solvothermal reaction. The obtained product was characterized by Powder XRD (Fig. 1b) and SEM (inset of Fig. 1b) which shows a needle-like shape. After comparing the XRD patterns of Ce-TCPP MOF with the patterns simulated from the single crystal structure of many TCPP MOFs, it seems that the structure of Ce-TCPP MOF did not agree with any of these single-phase MOFs. Instead, we found that the XRD patterns agree well with the combination of the XRD patterns from the crystal structure of VETTUK[10] and CAU-19 (Fig. 1b),[11] where the patterns of the former are more prominent. These results suggest that the crystalline structure of Ce-TCPP MOFs is dominated by the structure similar to VETTUK with slight contribution from CAU 19. The porosity of Ce-TCPP MOFs was confirmed by N_2 sorption measurement (Fig. S1) and Thermogravimetric Analysis (TGA) (Fig. S2). The average BET surface area is 342.67 m^2/g based on two measurements. This value is relatively small but within the range of literature results of similar TCPP based MOFs (330-600 $m^2\ g^{-1}$).[11] The TGA results show two characteristic steps, including a weight loss below 100°C and 360-500°C, which can be attributed to the evaporation of water molecules and the decomposition of MOF with the dissociation of Ce-O bond, respectively.[11] The formation of Ce-TCPP MOFs was further supported by the Fourier-transform infrared (FT-IR) spectroscopy (Fig. 1c), where we observed the disappearance of C=O stretching at 1700 cm^{-1} which is present in TCPP resulting from free -COOH, the shift of C=C valence vibration of phenyl rings from 1559 cm^{-1} to 1526 cm^{-1}, as well as the two new peaks at 1587 cm^{-1} and 1400 cm^{-1}, which can be assigned to asymmetric and symmetric vibrational stretching of COO^-, respectively.[12] These results together suggest the successful coordination of carboxyl group in TCPP with Ce metal ion in Ce-TCPP MOFs.

In addition to the bulk structure, the local coordination environment at Ce center in Ce-TCPP MOFs was confirmed by X-ray absorption spectroscopy (XAS). The X-ray absorption near edge structure (XANES) spectra of Ce-TCPP MOFs and two reference samples, i.e. hexagonal $CeCl_3\ 7H_2O$ (Ce^{3+}), cubic CeO_2 (Ce^{4+}), as well as the starting material $(NH_4)_2Ce(NO_3)_6$, are shown in Fig. 2a. The main feature at ~5725.5 eV in the spectrum of $CeCl_3$ is the absorption white line corresponding to the dipole allowed transition from Ce 2p to 5d mixed with $4f^1$ final state,[13] supporting that Ce in $CeCl_3$ has the trivalent state (Ce^{3+}). In contrast, XANES spectrum of CeO_2 and $(NH_4)_2Ce(NO_3)_6$ exhibits two distinct features, where the features for CeO_2 occur at ~5731 eV and 5737.5 eV and those for $(NH_4)_2Ce(NO_3)_6$ occur at 5729 eV and 5738 eV, which can be attributed to the mixed-valence behavior of tetravalent Cerium (Ce^{4+}) in its final state ($4f^15dt_{2g}L$ and $4f^05d$; L denotes the oxygen 2p hole).[14] Unlike the reference samples, the XANES spectrum of Ce-TCPP MOF shows the main absorption edge at 5725.5 eV and a weak feature at 5737.5 eV, which can be assigned to the $4f^1$ and $4f^0$ absorption peak, respectively, suggesting the co-existence of Ce^{3+}/Ce^{4+} valence state in Ce-TCPP MOF. This is further supported by the energy difference (~12 eV) between these two features, which agrees well with the Coulomb interaction of Ce 2p and Ce 4f orbitals.[15] As suggested by the previous literature report on similar Ce-MOFs,[11] Ce center in Ce-TCPP MOF is dominated by Ce^{3+} and can be attributed to the reduction of Ce^{4+} from the redox-active linkers (e.g. TCPP).

To gain deeper insight of the local coordination environment, we quantitatively fitted the extended X-ray absorption fine structure (EXAFS) spectrum of Ce-TCPP (Fig. S3a) using Demeter XAS analysis package. As the XRD results suggest that the structure of Ce-TCPP MOF is featured by the combination of VETTUK and CAU-19, the fitting models based on the crystal structure of both VETTUK[10] and CAU-19[11] were used to fit the data. It is interesting to note that the EXAFS spectrum can be adequately fit based on the crystal structure of VETTUK (fitting parameters listed in Table S1) but significant deviation was observed based on CAU-19. This can be explained by that the crystalline structure of Ce-TCPP MOF is dominated by the structure similar to VETTUK, which is consistent with XRD results. The EXAFS data and the resulting best fit in R-space and k-space are present in Fig. 2b and Fig. S3b, respectively. From the best fitting, the bond distance of Ce to O in Ce-TCPP was found to be between 2.22 Å to 2.61 Å. The Ce-O distances are within the range of distances reported in literature for Ce (IV) and Ce (III) cluster (2.206–2.234 Å for core Ce-O, 2.429 Å to 2.563 Å and 2.364 to 2.765 Å for the remaining Ce-O),[16] suggesting the validity of our fitting model.

Fig. 3a shows the UV-visible absorption spectrum of TCPP in methanol (black plot), the diffuse reflectance (DR) spectra of TCPP in solid state (blue plot) and Ce-TCPP MOFs (red plot). It was found that TCPP in methanol solution exhibits an intense Soret band centered at 415 nm (S_0-S_2 transition) and the relatively weaker Q bands (S_0-S_1 transition) which spread over a wide range in the visible region with four distinct peaks at 512 nm (Q_y), 547nm (Q_y), 588nm (Q_x) and 645nm (Q_x).[17] In contrast, Ce-TCPP MOFs show broad absorption extended to ~700 nm. This feature is likely due to scattering because it was also observed in the DR spectrum of TCPP in solid state. The Soret and Q bands of Ce-TCPP MOFs shows a prominent red-shift compared to TCPP, which can be attributed to the planarity change caused by deformation of TCPP during incorporation:

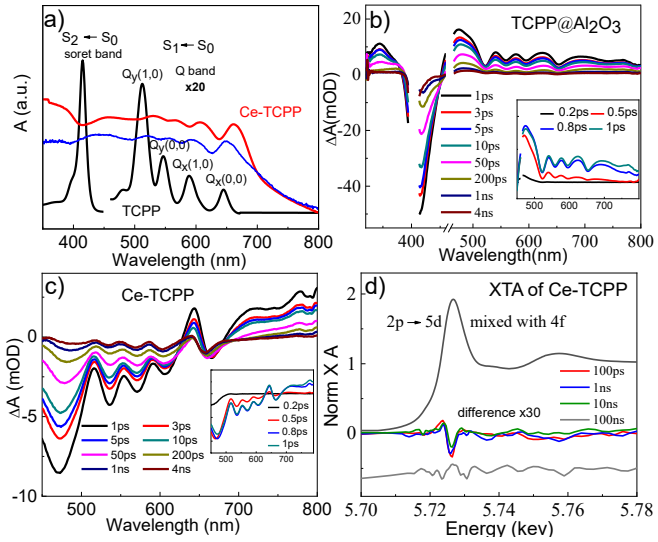

Figure 3. (a) UV-visible absorption spectrum of TCPP in methanol and the diffuse reflectance spectrum of TCPP in solid state (blue) and Ce-TCPP (red). OTA spectra of TCPP/Al_2O_3 (b) and Ce-TCPP (c) following 400 nm excitation. The insets show the early time OTA spectra. (d) XANES spectrum of Ce-TCPP MOFs at Ce L_3-edge (black plot) and the difference XANES spectra at 100 ps (red), 1ns (blue), 10ns (green), and 100 ns (gray) obtained by subtracting the laser-off spectrum from laser-on spectrum. The difference spectrum at 100 ns delay is shifted manually to have an offset for a clearer view.

the non-planarity confirmation of TCPP in Ce-TCPP MOF destabilizes the porphyrin HOMOs while the LUMOs were not affected significantly.[18] Moreover, the strong coupling of the well-arranged TCPP monomers (J-aggregation)[17b] may also contribute to the red-shift, which has been observed in other porphyrin- based MOFs reported previously.[19]

Femtosecond OTA spectroscopy was performed with selective excitation of TCPP Soret band to examine the excited state (ES) dynamics of Ce-TCPP MOFs. To better understand the effect of porous nature on ES dynamics in MOFs, we first measured the OTA spectra of TCPP on Al_2O_3 thin film, which represents a control sample for intrinsic ES dynamics of TCPP in heterogeneous environment. As shown in Fig. 3b and S4a, OTA spectra of TCPP/Al_2O_3 thin film consist of a negative band centered at 415 nm and a broad positive absorption feature from 450 nm overlapping with several distinct bleach signal at 520 nm, 563 nm, 596 nm and 653 nm. These features have been well studied and can be attributed to TCPP Soret band ground state bleach (GSB), ES absorption (ESA), and Q band GSB, respectively. The recovery of Soret GSB and the decay of ES follow the same kinetics (Fig. S4b), together with the presence of the isosbestic point at 451 nm, suggesting that the decay of ES molecules to their GS is the only relaxation process in TCPP/Al_2O_3 after excitation.

Compared to TCPP, the OTA spectra of Ce-TCPP MOFs are dramatically different. As shown in Fig. 3c, the OTA spectra of Ce-TCPP exhibit the Soret and Q band GSB with a red-shift in the range of 450 nm to 670 nm, which is consistent with its UV-visible ground state DR reflectance spectrum. However, the positive features pertaining to ESA are missing in the region < 600 nm even at early times (< 1 ps) (inset of Fig. 3c). We attribute this difference to the ultrafast (< 200 fs) formation of a new CS state evolved from singlet ES (i.e. S_2 & S_1) (Fig. S4c), as superfast CS was also observed for Q band excitation (Fig. S4d). The CS was further confirmed by the observation of the transient feature at > 700 nm region as the fingerprint absorption of one electron oxidized $TCPP^{*+}$.[20] These results, similar to previous reports accounting for electron transfer (ET) process in MOFs,[19, 21] implying that fast ET occurs from TCPP ligand to Ce metal cluster.

To gain more insight on the nature of CS state, we measured the OTA spectra of three reference samples including CAU-19, Ce based MOF that has the same crystal structure as VETTUK (denoted as Ce-VETTUK), as well as the physical mixture of these two MOFs. The details of the synthetic procedure and structural characterization (XRD, FTIR, DR spectrum, and XAS) of these two MOFs are presented in SI and Figure S5-S8. As shown in the OTA spectra of CAU-19 (Fig. S9a), Ce-VETTUK (Fig. S9b), and the physical mixture of both MOFs (Fig. S9c), these spectra largely look similar to that of TCPP/Al_2O_3, which consist of Soret GSB at < 480 nm, broad ESA, and multiple Q band GSB signals. However, it is notable that the Q band GSB bands, which remain positive in the spectra of TCPP/Al_2O_3 at all time delays, become negative in the spectra of CAU-19 at ~100 ps, Ce-VETTUK at ~50 ps, and the physical mixture of CAU-19 and Ce-VETTUK as early as 1 ps (Fig. S9 and S10). These results together suggest that CS state observed in mixed phase Ce-TCPP MOF also occurs in these reference samples, where the formation of CS is fastest in the mixed-phase Ce-TCPP, which then decreases following the order of the physical mixture of CAU-19 and Ce-VETTUK > Ce-VETTUK > CAU-19 (Fig. S11). These results suggest that the mixed-phase crystal structure in Ce-TCPP plays an important role in facilitating CS. While it remains unclear what the specific role of each phase plays, similar phase facilitated CS has been observed in other mixed-phase materials.[22] Nevertheless, we can conclude that the presence of long-lived CS state after ultrafast ET in the mixed-phase Ce-TCPP is expected to be beneficial for applications in photocatalysis.

To gain further insight on the nature of the long-lived CS in the mixed-phase Ce-TCPP, we directly probed the electron density changes at Ce center following selective excitation of TCPP ligand using XTA spectroscopy. Fig. 3d shows the XANES spectrum of Ce-TCPP at Ce L3 edge and the difference spectra obtained by subtracting the GS (laser-off) spectrum from spectrum collected at different delay times (100 ps, 1 ns, 10 ns and 100 ns) following 400 nm laser excitation. The positive feature observed at 5723.7 eV indicates that the edge energy of Ce shifts to lower energy, suggesting the formation of reduced Ce Center in Ce-TCPP. This is further supported by the negative feature observed at 5725.5 eV: the decreased number of empty 4f orbitals prohibits the excitation of 2p core electrons, resulting in the decreased absorption intensity. The intensity of this negative feature decreases gradually from 100 ps to 10 ns until 100 ns where no transient signal was observed, suggesting that this is a long-lived transient species (> 10 ns). These results together confirmed the formation of a long-lived CS state due to ligand-to-metal cluster charge transfer (LCCT) after photoexcitation of Ce-TCPP, consistent with OTA results above. As the Ce centers in Ce-TCPP is dominated by Ce^{3+} which is a stable oxidation state, the nature of the long-lived CS state is

likely the reduction of small fraction of Ce^{4+} by the TCPP ligands, which is similar to the mechanism of forming Ce^{3+} center in Ce-TCPP MOF from Ce^{4+} in starting material $(NH_4)_2Ce(NO_3)_6$.[23]

In summary, we have synthesized mixed-phase Ce-TCPP constructed from free-base TCPP ligand and Cerium ammonium nitrate. Using OTA spectroscopy, we show that ultrafast ET occurs from TCPP ligand to Ce center in Ce-TCPP MOFs following the excitation of TCPP ligand, forming a long-lived CS state. Systematic OTA studies on three control samples revealed that the presence of mixed-phase structure in Ce-TCPP MOF is responsible for the ultrafast formation of CS state. The nature of this CS state is featured by LCCT as confirmed by XTA, where the reduction of Ce center was observed due to excitation of TCPP ligand. The observed ultrafast charge transfer process which results into the formation of long-lived CS state (> 10 ns) is expected to be beneficial for photocatalysis and thus imply the potential application of Ce-TCPP MOFs in solar energy conversion.

This work was supported by National Science Foundation (CBET-1706971). Use of the Advanced Photon Source at Argonne National Laboratory was supported by the U. S. Department of Energy, Office of Science, Office of Basic Energy Sciences, under Award No. DE-AC02-06CH11357. Sizhuo Yang acknowledges the John J. Eisch fellowship during the 2018-2019 academic year.

Conflicts of interest

There are no conflicts to declare

Notes and references

1. (a) Aresta, M.; Dibenedetto, A.; Angelini, A., *Chem. Rev.* 2014, **114**, 1709-1742; (b) Sakakura, T.; Choi, J.-C.; Yasuda, H., *Chem. Rev.* 2007, **107**, 2365-2387.
2. (a) Moroz, P.; Royo Romero, L.; Zamkov, M., *Chem. Commun.* 2019, **55**, 3033-3048; (b) Ye, S.; Ding, C.; Liu, M.; Wang, A.; Huang, Q.; Li, C., *Adv. Mater.* 2019, **31**, 1902069; (c) Ye, S.; Ding, C.; Chen, R.; Fan, F.; Fu, P.; Yin, H.; Wang, X.; Wang, Z.; Du, P.; Li, C., *J. Am. Chem. Soc.* 2018, **140**, 3250-3256; (d) Kang, P.; Cheng, C.; Chen, Z.; Schauer, C. K.; Meyer, T. J.; Brookhart, M., *J. Am. Chem. Soc.* 2012, **134**, 5500-5503; (e) Hu, P.; Diskin-Posner, Y.; Ben-David, Y.; Milstein, D., *ACS Catal.* 2014, **4**, 2649-2652.
3. Furukawa, H.; Cordova, K. E.; O'Keeffe, M.; Yaghi, O. M., *Science* 2013, **341**, 974-+.
4. (a) Yang, S.; Pattengale, B.; Lee, S.; Huang, J., *ACS Energy Lett.* 2018, **3**, 532-539; (b) Wang, C.; Xie, Z.; deKrafft, K. E.; Lin, W., *J. Am. Chem. Soc.* 2011, **133**, 13445-13454; (c) Lammert, M.; Wharmby, M. T.; Smolders, S.; Bueken, B.; Lieb, A.; Lomachenko, K. A.; Vos, D. D.; Stock, N., *Chem. Commun.* 2015, **51**, 12578-12581.
5. (a) Dhakshinamoorthy, A.; Li, Z. H.; Garcia, H., *Chem. Soc. Rev.* 2018, **47**, 8134-8172; (b) Xiao, J.-D.; Jiang, H.-L., *Acc. Chem. Res.* 2019, **52**, 356-366.
6. (a) Kornienko, N.; Zhao, Y.; Kley, C. S.; Zhu, C.; Kim, D.; Lin, S.; Chang, C. J.; Yaghi, O. M.; Yang, P., *J. Am. Chem. Soc.* 2015, **137**, 14129-14135; (b) Li, R.; Zhang, W.; Zhou, K., *Adv. Mater.* 2018, **30**, 31; (c) Rice, A. M.; Leith, G. A.; Ejegbavwo, O. A.; Dolgopolova, E. A.; Shustova, N. B., *ACS Energy Lett.* 2019, **4**, 1938-1946.
7. (a) Hanna, L.; Kucheryavy, P.; Liu, C.; Zhang, X.; Lockard, J. V., *J. Phys. Chem. C* 2017, **121**, 13570-13576; (b) Shaikh, S. M.; Chakraborty, A.; Alatis, J.; Cai, M.; Danilov, E.; Morris, A. J., *Faraday Discuss.* 2019, **216**, 174-190.
8. (a) Hanna, L.; Long, C. L.; Zhang, X.; Lockard, J. V., *Chem. Commun.* 2020; (b) Caballero-Mancebo, E.; Cohen, B.; Smolders, S.; De Vos, D. E.; Douhal, A., *Adv. Sci.* 2019, **6**, 1901020; (c) Yu, J.; Park, J.; Van Wyk, A.; Rumbles, G.; Deria, P., *J. Am. Chem. Soc.* 2018, **140**, 10488-10496; (d) Alvaro, M.; Carbonell, E.; Ferrer, B.; Llabrés i Xamena, F. X.; Garcia, H., *Eur. J. Chem.* 2007, **13**, 5106-5112; (e) de Miguel, M.; Ragon, F.; Devic, T.; Serre, C.; Horcajada, P.; García, H., *ChemPhysChem* 2012, **13**, 3651-3654.
9. Pattengale, B.; Yang, S.; Ludwig, J.; Huang, Z.; Zhang, X.; Huang, J., *J. Am. Chem. Soc.* 2016, **138**, 8072-8075.
10. George, S.; Lipstman, S.; Goldberg, I., *Cryst. Growth Des.* 2006, **6**, 2651-2654.
11. Rhauderwiek, T.; Heidenreich, N.; Reinsch, H.; Oien-Odegaard, S.; Lomachenko, K. A.; Rutt, U.; Soldatov, A. V.; Lillerud, K. P.; Stock, N., *Cryst. Growth Des.* 2017, **17**, 3462-3474.
12. Lin, A.; Ibrahim, A. A.; Arab, P.; El-Kaderi, H. M.; El-Shall, M. S., *ACS Appl. Mater. Interfaces* 2017, **9**, 17961-17968.
13. Sugimoto, T.; Joseph, B.; Paris, E.; Iadecola, A.; Mizokawa, T.; Demura, S.; Mizuguchi, Y.; Takano, Y.; Saini, N. L., *Phys. Rev. B* 2014, **89**.
14. Jacobs, G.; Patterson, P. M.; Williams, L.; Chenu, E.; Sparks, D.; Thomas, G.; Davis, B. H., *APPL. CATAL. A-GEN.* 2004, **262**, 177-187.
15. (a) Thole, B. T.; Vanderlaan, G.; Fuggle, J. C.; Sawatzky, G. A.; Karnatak, R. C.; Esteva, J. M., *Phys. Rev. B* 1985, **32**, 5107-5118; (b) Kotani, A.; Kvashnina, K. O.; Glatzel, P.; Parlebas, J. C.; Schmerber, G., *Phys. Rev. Lett.* 2012, **108**, 5.
16. (a) Mathey, L.; Paul, M.; Coperet, C.; Tsurugi, H.; Mashima, K., *Chem.: Eur. J* 2015, **21**, 13454-13461; (b) Das, R.; Sarma, R.; Baruah, J. B., *Inorg. Chem. Commun.* 2010, **13**, 793-795.
17. (a) Venkatesh, Y.; Venkatesan, M.; Ramakrishna, B.; Bangal, P. R., *J. Phys. Chem. B* 2016, **120**, 9410-9421; (b) McCarthy, B. D.; Hontz, E. R.; Yost, S. R.; Van Voorhis, T.; Dincă, M., *J. Phys. Chem. Lett.* 2013, **4**, 453-458.
18. (a) Parusel, A. B. J.; Wondimagegn, T.; Ghosh, A., *J. Am. Chem. Soc.* 2000, **122**, 6371-6374; (b) Haddad, R. E.; Gazeau, S.; Pecaut, J.; Marchon, J. C.; Medforth, C. J.; Shelnutt, J. A., *J. Am. Chem. Soc.* 2003, **125**, 1253-1268.
19. Li, X. X.; Gong, C. H.; Gurzadyan, G. G.; Gelin, M. F.; Liu, J. X.; Sun, L. C., *J. Phys. Chem. C* 2018, **122**, 50-61.
20. (a) Harriman, A., *J. Chem. Soc. Faraday Trans.* 1981, **77**, 1281-1291; (b) Keane, P. M.; Kelly, J. M., *Photochem. Photobiol. Sci.* 2011, **10**, 1578-1586.
21. Gutierrez, M.; Cohen, B.; Sanchez, F.; Douhal, A., *Phys. Chem. Chem. Phys.* 2016, **18**, 27761-27774.
22. (a) Li, A.; Wang, Z.; Yin, H.; Wang, S.; Yan, P.; Huang, B.; Wang, X.; Li, R.; Zong, X.; Han, H.; Li, C., *Chem. Sci.* 2016, **7**, 6076-6082; (b) Rodríguez, N. A.; Parra, R.; Grela, M. A., *RSC Adv.* 2015, **5**, 73112-73118; (c) Henning, A.; Sangwan, V. K.; Bergeron, H.; Balla, I.; Sun, Z.; Hersam, M. C.; Lauhon, L. J., *ACS Appl. Mater. Interfaces* 2018, **10**, 16760-16767; (d) Ferron, T.; Waldrip, M.; Pope, M.; Collins, B. A., *J. Mater. Chem. A* 2019, **7**, 4536-4548.
23. (a) Cerium and Cerium Compounds. In *Kirk‐Othmer Encyclopedia of Chemical Technology*, pp 1-23; (b) Schelter, E. J., *Nat. Chem.* 2013, **5**, 348-348.

